Design and Control of a Miniature Bipedal Robot with Proprioceptive Actuation for Dynamic Behaviors

Yeting Liu[1], Junjie Shen[1], Jingwen Zhang[1], Xiaoguang Zhang[1], Taoyuanmin Zhu[1], and Dennis Hong[1]

***Abstract*— As the study of humanoid robots becomes a worldwide interdisciplinary research field, the demand for a cost-effective bipedal robot system capable of dynamic behaviors is growing exponentially. This paper presents a miniature bipedal robot named Bipedal Robot Unit with Compliance Enhanced (BRUCE). Each leg of BRUCE has five degrees of freedom (DoFs), which includes a spherical hip joint, a knee joint, and an ankle joint. To lower the leg inertia, a cable-driven differential pulley system and a linkage mechanism are applied to the hip and ankle joints, respectively. With the proposed design, BRUCE is able to achieve a similar range of motion to a human's lower body. The proprioceptive actuation and contact sensing further prepare BRUCE for interactions with unstructured environments. For real-time control of dynamic motions, a convex formulation for model hierarchy predictive control (MHPC) is introduced. MHPC plans with whole-body dynamics in the near horizon and simplified dynamics in the long horizon to benefit from both model accuracy and computational efficiency. A series of experiments were conducted to evaluate the overall system performance including hip joint analysis, walking, push recovery, and vertical jumping.**

I. Introduction

Ever since the creation of the first humanoid robot, the P series by Honda [1], humanoid robots have been developed in various aspects such as joint design with high precision and torque, integration of sensors and computer vision to sense the environment, as well as software and control algorithms. However, dynamic behaviors such as running and jumping remain challenging for humanoid robots. One of the main problems is the lack of capability to properly handle contact impact due to the high gear ratio of traditional servo motors. Series elastic actuators (SEAs) provide a great potential solution to this, but they can still suffer from the low force control bandwidth [2], [3]. Recently, proprioceptive actuation has exerted huge influence on robotics due to its impact mitigation and wide-bandwidth force control capabilities [4]. With proprioceptive actuators, highly dynamic motions have become feasible for quadruped robots [5], [6], but few examples exist for humanoid robots.

A. Humanoid Robot Platform

The main reason for the slower development in humanoid robots than quadruped robots in terms of dynamic behaviors lies not only on more complex control algorithms but also on the limited accessibility to hardware. Atlas from Boston Dynamics [7] is proved to be the most dynamic full-size humanoid robot with advanced control algorithms and state-of-the-art hardware. However, its accessibility is highly restricted. Digit from Agility Robotics [8] is also a great humanoid robot platform that addresses the mobility limitations of conventional humanoids, but it costs over 250,000 USD per unit. In terms of accessibility, the small-size humanoid robots seem to be a more preferable option for research purposes. DarwIn-OP by RoMeLa [9] has been a reliable open-platform humanoid robot due to its great performance and affordable price. Although traditional servo motors are used in DarwIn-OP for actuation, it still presents better dynamic performance than regular full-size humanoid robots thanks to its reduced size and moment of inertia. In order to promote highly dynamic motion development for humanoid robots, a miniature bipedal robot with proprioceptive actuation is thus desired.

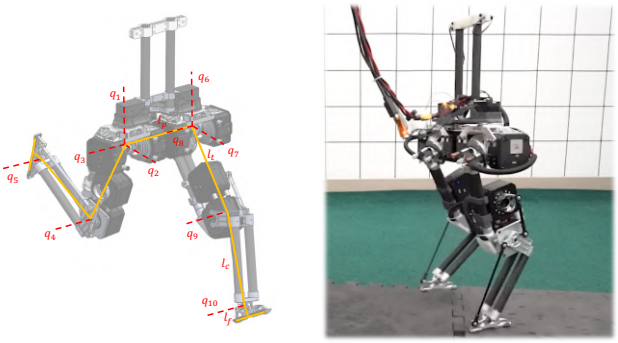

Fig. 1. Bipedal Robot Unit with Compliance Enhanced (BRUCE). On the left is the CAD model and on the right is the hardware platform during open-loop LIPM walking.

Inspired by the accessibility and reliability of current small-size humanoid robot platforms, as well as the rising technology of proprioceptive actuation, we have been developing the next-generation miniature Bipedal Robot Unit with Compliance Enhanced (BRUCE) as shown in Fig. 1. In order to perform human-like dynamic motions, the joint configuration and range of motion are designed to be close to that of human beings as seen in Fig. 2. Unlike the traditional humanoid robots whose actuators are directly located at each joint, a 2-DoF cable-driven differential pulley system and a 4-bar linkage mechanism are applied to the hip and ankle joints, respectively. By doing so, the moment of inertia of each leg is significantly reduced in favor of highly dynamic leg motions. Meanwhile, the choice of cable drive for the differential transmission also brings less backlash than conventional bevel gears.

[1]Yeting Liu, Junjie Shen, Jingwen Zhang, Xiaoguang Zhang, Taoyuanmin Zhu, and Dennis Hong are with the Robotics and Mechanisms Laboratory, the Department of Mechanical and Aerospace Engineering, University of California, Los Angeles, CA 90095, USA {liu1995, junjieshen, zhjwzhang, hawkblizzard, tymzhu, dennishong}@ucla.edu

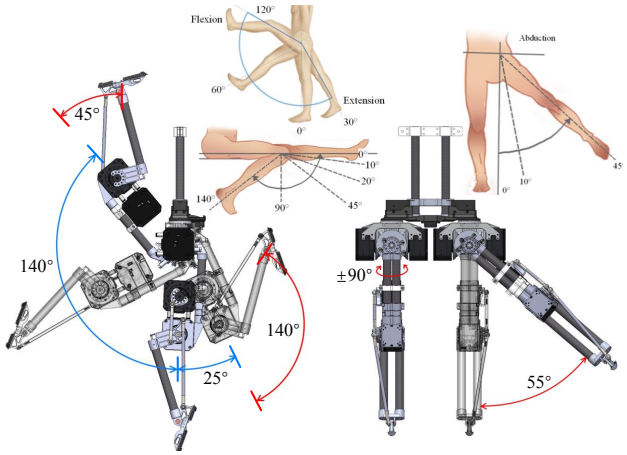

Fig. 2. Lower body comparison of joint configuration and range of motion between BRUCE and human being [10].

B. Model Predictive Control

Model predictive control (MPC) has been proven an effective approach in dynamic legged motion studies. It considers solving a trajectory optimization problem in real time, which determines the control sequences over a receding prediction horizon into the future. There are mainly two categories, simple-model and whole-body MPCs. Simple-model MPC generates a low-dimensional plan which is then tracked by a whole-body controller. Commonly used simple models include the linear inverted pendulum model (LIPM) [11]–[14], centroidal momentum model [15]–[17], and single rigid body model [6], [18]–[22]. Simple-model MPC can execute in real time at high rates. Nonetheless, an oversimplified model would limit the robot's motion capability and additional details need to be separately designed, e.g., swing leg motion, which not only increases complexity but could also possibly fight against the plan [19]. By comparison, whole-body MPC can exploit every single detail of the robot and produce more intricate behaviors [23], [24]. However, due to the complexity of high-dimensional models, these problems, usually formulated as a nonlinear program (NLP), are still computationally expensive, suffer from initial guess and local minima issues, and sometimes even end up being intractable [25]–[29]. Recently, a new approach called model hierarchy predictive control (MHPC) [30] is introduced. MHPC plans with full-body model in the near horizon and simple model in the long horizon to benefit from both model accuracy and computational efficiency. Nevertheless, nonlinear MHPC is still of considerable computational complexity and cannot be executed online even for planar legged systems [30]. In this paper, we propose a convex formulation for MHPC, which can be solved efficiently for general 3D scenarios and implemented in real time for feedback control.

C. Contribution

1) Design: BRUCE, a next-generation miniature bipedal robot, is presented as an accessible and reliable humanoid platform for research purposes. The cable-driven differential pulley system and linkage mechanism are designed for reducing leg inertia in favor of dynamic behaviors while proprioceptive actuation and contact sensing further prepare BRUCE for interactions with unstructured environments.

2) Control: A convex formulation of MHPC is proposed to address the common issues of NLP, e.g., local minima and slow solving speed. Implementation of convex MHPC on BRUCE for push recovery, center of mass (CoM) tracking, and vertical jumping, can achieve a processing frequency of 250 Hz, which is sufficient for real-time whole-body control.

TABLE I

BRUCE MECHANICAL PARAMETERS

Parameter	Value [Unit]	Parameter	Value [Unit]
Body mass m_b	315 [g]	Total mass m	3,567 [g]
Hip mass m_h	667 [g]	Pelvis length l_p	150 [mm]
Thigh mass m_t	839 [g]	Thigh length l_t	175 [mm]
Calf mass m_c	96 [g]	Calf length l_c	169.5 [mm]
Foot mass m_f	24 [g]	Foot length l_f	24 [mm]

TABLE II

KOALA BEAR SPECIFICATIONS

Weight	Speed Constant	Torque Constant
250 [g]	27.3 [RPM/V]	0.35 [Nm/A]
Gear Ratio	**Stall Torque (15 sec)**	**Stall Torque (1.5 sec)**
9	3.5 [Nm]	10.5 [Nm]

II. DESIGN OF BRUCE

A. Mechanical Configuration

1) Joint Configuration: To ensure BRUCE has an adequate range of motion while keeping the overall platform simple and lightweight, each leg is composed of a spherical hip joint, a single DoF knee joint, and a single DoF ankle joint, as shown in Fig. 1. Moreover, each foot has a line contact with the ground so that the actuation in the foot roll direction can be omitted. Unlike regular full-size humanoid robots with fully actuated ankles, the single DoF ankles in BRUCE could lose some foot functionality. Nevertheless, the benefit from the lightweight design outweighs this drawback distinctly when it comes to highly dynamic leg motions.

2) Link Length: BRUCE is designed to be a miniature bipedal robot with a similar range of motion to that of a human's lower body. Therefore, the size of BRUCE is scaled down from a full-size human. The total height of BRUCE is 660 mm. The link lengths of its upper body, thigh, calf, and foot are respectively 291.5 mm, 175 mm, 169.5 mm, and 24 mm, which results in a similar length ratio to that of an average adult [31]. The distance between legs is 150 mm to prevent collision between the hip actuators. Table. I lists the major mechanical parameters of BRUCE.

B. Actuation Scheme

In order to have better actuation transparency and compliance to unstructured environments, Koala BEAR proprioceptive actuators [32] from Westwood Robotics [33] are adopted. The actuator specifications can be found in Table II. The hip yaw joints are currently powered by traditional servo motors since they do not require much compliance, which also reduces the overall weight and saves the budget.

With this proprioceptive actuation scheme, BRUCE's legs are desired to have low inertia in favor of dynamic behaviors.

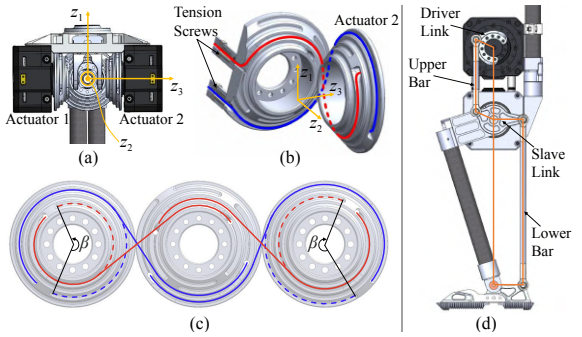

Fig. 3. BRUCE leg design highlights: (a) Spherical hip joint, (b) Assembly of pulleys and cables pretensioned by screws, (c) Wiring schematic of 2-DoF cable-driven differential pulley system, where β represents the effective rotation region for the pulley which also corresponds to the range of hip roll motion, and (d) Linkage mechanism for ankle joint actuation.

The distribution of the actuators needs to be reconsidered so that they can be kept close to the torso instead of being directly located at each joint like traditional humanoid robots. In the past, researchers have proposed some reliable solutions by using cable-driven systems [34], [35] and linkage mechanisms [36]. Inspired by previous work, a 2-DoF cable-driven differential pulley system is designed for the hip pitch and roll motions, and two pairs of 4-bar linkage mechanisms are used to actuate the ankle joint.

C. Hip Design With Cable-Driven System

Instead of connecting two actuators in serial for the pitch and roll joints of hip, a 2-DoF parallel actuation configuration is preferable for BRUCE. First, this design could mount the two actuators on the hip to reduce the mass and inertia of the femur link. Moreover, the available hip pitch torque is doubled as the two actuators are powering the same joint, which could benefit BRUCE during dynamic motions in the sagittal plane, as is usually the case.

Previously, the prototype of BRUCE [10] was using bevel gears to realize the parallel actuation scheme of the hip. However, the leg wobbled easily, and hip joint accuracy was low due to the backlash in gears as shown in the supplementary video. To improve the joint accuracy and stability, the compact cable transmission with cable differential [37] is novelly applied on the hip joint to form a cable-driven differential pulley system, which has already been successfully implemented on other robotic joints such as the torso [38] and shoulder [39]. Despite the extra complexity in installation, the cable-driven differential pulley system appears to be a suitable replacement for traditional bevel gears due to its zero-backlash feature. In addition, unlike gears in which grease is necessary for lubrication, no lubrication is needed between the cable and pulley, which could be beneficial to the cleanliness of the hip assembly.

The proposed 2-DoF cable-driven differential pulley system is illustrated in Fig. 3a-3c. To effectively actuate the hip joint in both pitch and roll directions without slip, at least two cables are needed for each pulley attached to the hip actuator, and it results in a total of four cables for the pulley connected to the femur link. As shown in Fig.3b, the blue cable is active when Actuator 2 rotates along positive z_3 direction, while the reverse rotation will make the red cable active. To avoid any broken cables due to the excessive load, the minimum radius R_{min} of wrapping the cable around the pulley needs to be carefully determined, which is related to the maximum torque of the actuator T_{max} and the material property for the cable as follows:

$$R_{\text{min}} = T/F_y \leq T_{\text{max}}/F_y = T_{\text{max}}/\left(\sigma_y \cdot \pi r_c^2\right), \qquad (1)$$

where σ_y is the yield stress of the cable material, and r_c is the radius of the cable. In our case, with $T_{\text{max}} = 10.5$ Nm for the actuator, $\sigma_y = 215$ MPa and $r_c = 2.4$ mm for a 304 stainless steel cable, the maximum of R_{min} is determined to be 16.2 mm for a safety factor of 1.5. On the real hardware, it is adjusted to 19 mm to properly fit into the assembly.

The parallel configuration of the hip joint in the pitch and roll directions leads to the coupling of the two actuators. As illustrated in Fig.3b and 3c, pure hip pitch motion will be achieved when the two side pulleys rotate for the same angle in the opposite directions, while rotating in the same direction leads to pure roll motion. Any other rotations will lead to both pitch and roll motions simultaneously.

TABLE III
BRUCE ANKLE JOINT RANGE OF MOTION

Knee Angle*	-30°	0°	30°	60°	90°	120°
Min. Ankle Angle†	-25°	-60°	-58°	-58°	-58°	-58°
Max. Ankle Angle†	77°	72°	50°	28°	-3°	-32°

*We define the positive direction as the knee flexes.
†The ankle angle is 0° when the foot is perpendicular to the tibia, and the positive direction is defined as the foot flexes.

D. Leg Design With Linkage Mechanism

The femur and tibia linkages of BRUCE are composed of carbon fiber tubes and topology-optimized aluminium parts. The two actuators for the knee and ankle joints are mounted in the femur link to keep the tibia link as light as possible. Since the ankle actuator is relocated to the femur link, a mechanism to transmit the torque from the actuator to the ankle joint is needed. Generally, timing belt is a good option for power transmission due to its simplicity and the ability to transmit continuous rotations. However, due to its low stiffness, there will be unwanted compliance between the belt teeth and pulley. As a result, the rotor-belt resonant frequency will be low, which could limit the torque control bandwidth of the joint [40]. To overcome this problem, a reliable torque transmission with high stiffness is used, i.e., linkage mechanism.

As shown in Fig. 3d, BRUCE utilizes two pairs of 4-bar linkage mechanisms both of parallelogram configuration to properly transmit the torque from the actuator to the ankle joint with a 1:1 transmission ratio. Since the lower bar is such a thin and long link, the buckling load F_{buckling} verification must be done to determine its radius r_l so that it will not buckle under extreme scenarios as follows:

$$F_{\text{buckling}} = \pi^2 E_l I / L_l^2 \geq T_{\text{max}}/l, \qquad (2)$$

where E_l, I, L_l, l are the Young's Modulus for the lower bar material, moment of inertia of the cross section of the lower

Fig. 4. BRUCE contact sensing foot. On the left is the exploded view of the CAD model and on the right is the hardware assembly.

bar, the length of lower bar, and the moment arm of the slave link. To match with the tibia link length, we need to use a 169.5 mm long aluminum rod with $E_l = 6.9 \times 10^{10}$ N/m^2 and $I = \pi r_l^2/4$. With $T_{\max} = 10.5$ Nm for the actuator and $l = 30$ mm, (2) will lead to the minimum radius of 3 mm for the lower bar with a safety factor of 1.5. Moreover, due to the complexity of the two linkage mechanisms, the ankle joint motion depends on the knee configuration. Table. III lists the ankle joint range with varying knee angles.

E. Contact Sensing Foot

A reliable yet lightweight contact sensing foot module is proposed for BRUCE, as shown in Fig. 4, in order for BRUCE being able to detect when the contact between the foot and the ground is created or broken for state estimation purpose in an unstructured environment. The sensing foot is designed based on the working principle of an electronic switch. When the foot is touching the ground, the plastic contact layer will bend and make the copper foils touch the aluminum base to close the circuit. Meanwhile, there is a potential false positive contact detection when the leg is swinging in the air with a large acceleration since the plastic contact layer can possibly deform due to inertia. However, while the contact layer weighs only 1.5 g, the required acceleration to trigger that false positive detection is computed to be about 80 and 166 times gravitational acceleration for the toe and heel, respectively, which far exceeds the normal operating condition for BRUCE.

III. Software and Control

To make BRUCE favorable to dynamic behaviors which require fast response, the overall software framework is developed in a multithreaded environment, which includes a motor communication thread, a state estimation thread combined with robot model computation, and a feedback control thread. The control thread is using the proposed convex MHPC, which replans trajectories and determines optimal torque commands in real time at a rate of 250 Hz. The main advantage of multithreading is that the idle time of CPU can be kept to minimum since the waiting time for sensor response can be well distributed and utilized. Data communication utilizes a custom shared memory library as illustrated in Fig. 5, similar to the setup developed in [41]. All programs are implemented in Python while some parts, including kinematics, dynamics [42], and state estimation [43], are precompiled using Numba [44] for acceleration.

The proposed convex MHPC is illustrated in Fig. 6, which

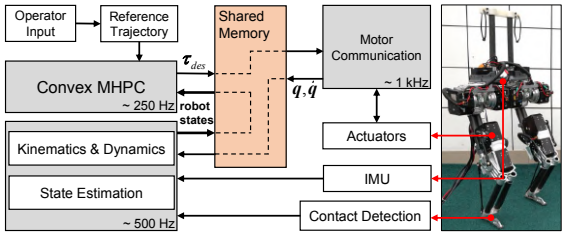

Fig. 5. Software architecture block diagram. The shaded blocks are run in separate threads and signals are communicated between them using shared memory. The proposed convex MHPC solves real-time control commands using the current robot states from the state estimator.

is formulated as a quadratic program (QP) as follows:

$$\min_{\substack{\ddot{\boldsymbol{q}},\boldsymbol{F}_i,\\ \boldsymbol{x}_k,\boldsymbol{u}_k}} \; J_t + \sum_{k=1}^{N_s} \|\boldsymbol{x}_k - \boldsymbol{x}_{d,k}\|^2_{\boldsymbol{Q}_k} + \sum_{k=1}^{N_s-1} \|\boldsymbol{u}_k\|^2_{\boldsymbol{R}_k} \tag{3a}$$

$$\text{s.t.} \;\; \boldsymbol{S}_f\left(\boldsymbol{H}\ddot{\boldsymbol{q}} + \boldsymbol{C}\dot{\boldsymbol{q}} + \boldsymbol{G} - \sum_{i=1}^{N_c} \boldsymbol{J}_{c_i}^\top \boldsymbol{F}_i\right) = \boldsymbol{0}, \tag{3b}$$

$$\boldsymbol{\tau}_{\min} \le \boldsymbol{\tau} \le \boldsymbol{\tau}_{\max}, \tag{3c}$$

$$\boldsymbol{J}_{c_i}\ddot{\boldsymbol{q}} + \dot{\boldsymbol{J}}_{c_i}\dot{\boldsymbol{q}} = \boldsymbol{0}, \;\; i = 1,\dots,N_c, \tag{3d}$$

$$\boldsymbol{F}_i \in \boldsymbol{\mathcal{C}}_i, \;\; i = 1,\dots,N_c, \tag{3e}$$

$$\boldsymbol{x}_{k+1} = \boldsymbol{A}\boldsymbol{x}_k + \boldsymbol{B}\boldsymbol{u}_k + \boldsymbol{d}, \;\; k = 1,\dots,N_s-1, \tag{3f}$$

$$\boldsymbol{f}_{i,k} \in \boldsymbol{\mathcal{C}}_{i,k}, \;\; i = 1,\dots,N_c, \; k = 1,\dots,N_s-1, \tag{3g}$$

$$\boldsymbol{h}_1 = \boldsymbol{h} + \dot{\boldsymbol{h}}\Delta t, \;\; \boldsymbol{p}_1 = \boldsymbol{p} + \boldsymbol{l}_1 \Delta t/m. \tag{3h}$$

MHPC plans with full-body model in the near horizon (3b-3e), simple model in the long horizon (3f-3g), as well as model transition (3h) in between to enforce consistency. The cost function is also a combination of objectives for both models. To make the formulation convex and tractable, the full-body model is only considered for the very first time step, and the simple model is also linearized around the operating point. Let us now go over the details.

1) Full-Body Model: The joint-space dynamic equations of motion for a legged system is in the form of

$$\boldsymbol{H}\ddot{\boldsymbol{q}} + \boldsymbol{C}\dot{\boldsymbol{q}} + \boldsymbol{G} = \boldsymbol{S}_a^\top \boldsymbol{\tau} + \sum_{i=1}^{N_c} \boldsymbol{J}_{c_i}^\top \boldsymbol{F}_i, \tag{4}$$

where $\boldsymbol{q}$, $\boldsymbol{H}$, $\boldsymbol{C}\dot{\boldsymbol{q}}$, $\boldsymbol{G}$, $\boldsymbol{S}_a$, $\boldsymbol{\tau}$ are the familiar generalized coordinates including the 6-DoF floating base joint, inertia matrix, Coriolis and centrifugal force, gravity force, actuation selection matrix, and actuation torque. $\boldsymbol{J}_{c_i}$ and $\boldsymbol{F}_i$ are the foot contact Jacobian and contact force for the ith contact vertex. N_c is the number of total contact vertices. To accelerate the optimization performance, variables for $\boldsymbol{\tau}$ are removed and expressed as a function of $\ddot{\boldsymbol{q}}$ and $\boldsymbol{F}_i$ in (3c) and only the floating base dynamics are considered as (3b), where $\boldsymbol{S}_f$ is the base selection matrix. The constraint (3d) ensures the contact foot does not move while (3e) ensures the contact force is bounded and lies within the local friction cone $\boldsymbol{\mathcal{C}}$, which is approximated by a square pyramid [45]. Finally, the first term in the cost function (3a) describes all the operational-space tasks with weighted priorities as follows:

$$J_t = \sum_{j=1}^{N_t} \left\| \boldsymbol{J}_{t_j}\ddot{\boldsymbol{q}} + \dot{\boldsymbol{J}}_{t_j}\dot{\boldsymbol{q}} - \boldsymbol{a}_{d,j} \right\|^2_{\boldsymbol{W}_j}, \tag{5}$$

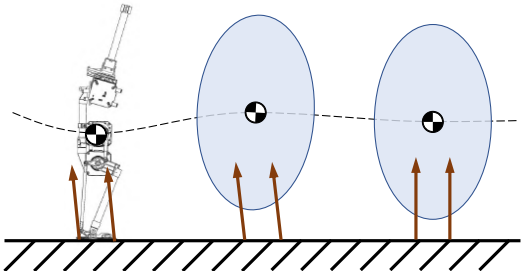

Fig. 6. Illustration of the convex MHPC framework. MHPC plans with robot full-body model for the first time step and simple model in the long horizon to benefit from both model accuracy and computational efficiency.

where $\boldsymbol{J}_{t_j}$, $\boldsymbol{a}_{d,j}$, and $\boldsymbol{W}_j$ are respectively the task Jacobian, desired acceleration, and weight for the jth task, e.g., body posture, swing leg motion. N_t is the number of total tasks. Note that the weighted vector norm square is defined as $\|\boldsymbol{e}\|^2_{\boldsymbol{W}} := \boldsymbol{e}^\top \boldsymbol{W} \boldsymbol{e}$ for $\boldsymbol{e} \in \mathbb{R}^n$ and $\boldsymbol{W} \in \mathbb{S}^n_+$.

2) Simple Model: The centroidal momentum dynamics is utilized as the simple model in this framework as follows:

$$\dot{\boldsymbol{l}} = m\ddot{\boldsymbol{p}} = m\boldsymbol{g} + \sum_{i=1}^{N_c} \boldsymbol{f}_i, \quad \dot{\boldsymbol{k}} = \sum_{i=1}^{N_c} \boldsymbol{r}_i \times \boldsymbol{f}_i, \tag{6}$$

where $\boldsymbol{p}$ is the CoM position, $\boldsymbol{h} := \left[\boldsymbol{l}^\top, \boldsymbol{k}^\top\right]^\top$ is the centroidal momentum including both linear and angular parts, $\boldsymbol{f}_i$ and $\boldsymbol{r}_i$ are the contact force and position vector of the ith contact vertex relative to CoM, m is the robot mass and $\boldsymbol{g}$ is the gravity vector. The cross product $\boldsymbol{r}_i \times \boldsymbol{f}_i$ will bring about nonlinearity into the formulation. To linearize this term, assume $\boldsymbol{r}_i$ will not change substantially under well-controlled motions, and thus, it is set to the current value and held fixed throughout the prediction horizon. Note that although the robot model will deviate, it is always correct for the first time step, and MHPC can also execute at a sufficiently high frequency, preventing it from divergence due to this rough approximation. Denote the linearized system state as $\boldsymbol{x} := \left[\boldsymbol{p}^\top, \boldsymbol{h}^\top\right]^\top$ with control input as $\boldsymbol{u} = \left[\boldsymbol{f}_1^\top, \ldots, \boldsymbol{f}_{N_c}^\top\right]^\top$, the momentum dynamics (6) can be discretized with sampling period Δt and further rewritten in its state-space form as (3f), where N_s is the number of total time steps. Similar to (3e), the contact force constraint is also enforced as (3g). Finally, the second part of the cost function (3a) will be minimized in terms of overall tracking error and control effort in the least-squares sense for the simple model.

3) Model Transition: With the two models separately formulated, the last step is to connect their states at transition. For the full-body model, the centroidal momentum matrix [46] $\boldsymbol{A}_G$ relates the generalized acceleration $\ddot{\boldsymbol{q}}$ to the change rate of the centroidal momentum $\dot{\boldsymbol{h}}$ as follows:

$$\dot{\boldsymbol{h}} = \boldsymbol{A}_G \ddot{\boldsymbol{q}} + \dot{\boldsymbol{A}}_G \dot{\boldsymbol{q}}. \tag{7}$$

As a result, given the current value of $\boldsymbol{h}$ and $\boldsymbol{p}$, integrating once with respect to time will get us the next $\boldsymbol{h}_1$ and a second integration of the linear part will get us the next $\boldsymbol{p}_1$ as (3h).

IV. Performance Evaluation

This section evaluates the overall performance of BRUCE with different tests, including hip joint analysis, kinematics verification, and proposed convex MHPC evaluation. Experimental results are discussed and more information can be seen in the supplementary video.

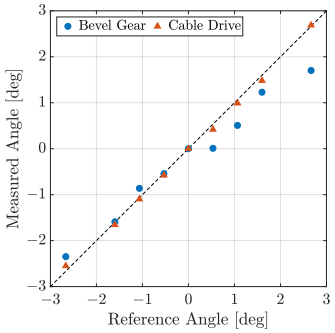

Fig. 7. Hip joint backlash comparison between the cable-driven differential pulley system and the differential bevel gear system.

A. Hip Joint Backlash and Stiffness

To show the cable-driven differential pulley system has far less backlash than the traditional differential bevel gear system, a comparison experiment was conducted to visualize the two backlash conditions. For test setup, two hip assemblies with different designs were mounted to a fixed location respectively, and a background paper was placed behind with reference points on it. For data collection, the thigh link in each assembly was manually aligned to the reference points, and the angle readings from the two hip actuators were recorded for comparison. The result is shown in Fig. 7 and we can see that the measured angles from the cable-driven hip joint almost perfectly fit the reference while the bevel gear hip module has a poorer performance.

Furthermore, as the cable-driven transmission is applied to the hip joint, the joint stiffness needs to be analyzed since it might be affected by the cable elongation. The cable axial stiffness k_c can be first determined to be

$$k_c = AE_c/L_c = \pi r_c^2 \cdot E_c/(2\pi R) = 0.5 r_c^2 E_c/R. \tag{8}$$

where A, L_c are the cross-sectional area and the length of the cable, and E_c is the Young's Modulus for the cable material. The joint stiffness k_j can then be determined to be

$$k_j = T/\Delta\theta = FR/(\delta/R) = k_c R^2 = 0.5 r_c^2 E_c R, \tag{9}$$

where $\delta = F/k_c$ is the cable elongation and $\Delta\theta$ is the resultant joint rotation angle. With $R = 19$ mm for the pulley, $r_c = 2.4$ mm and $E_c = 1.9 \times 10^{11}$ N/m^2 for the 304 stainless steel cable, the hip joint stiffness is 10,397 Nm/rad, which is sufficiently stiff as the actuator only has a maximum torque of 10.5 Nm. The resultant joint rotation due to cable elongation is $0.058°$ at worst, which is negligible. In addition, each cable is properly pretensioned by adjusting the screws in Fig. 3b to ensure reliable power transmission.

B. Kinematics Verification

To verify the kinematics, a seesaw balancing test was first conducted. Ideally an IMU should be mounted on the seesaw so that the ground information is accessible, and BRUCE can keep its body pose using position control based on inverse

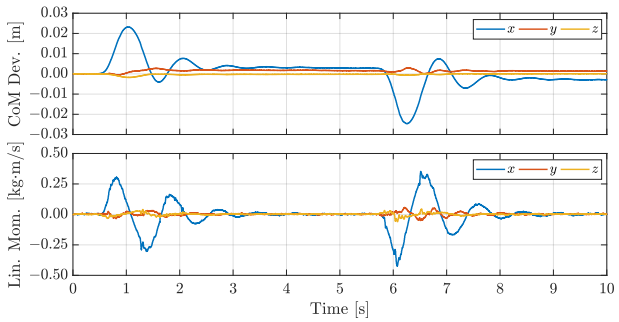

Fig. 8. Experimental results of push recovery in the x direction. The figure shows the time history of CoM deviation from its initial position and linear momentum in each direction.

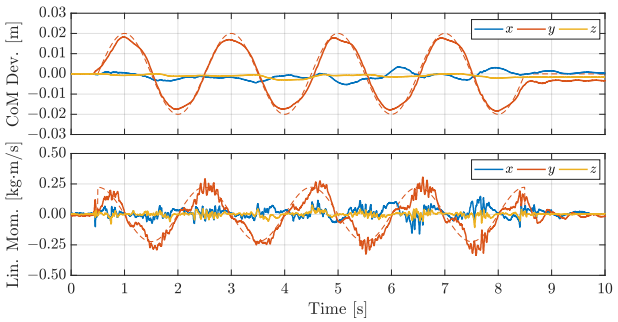

Fig. 9. Experimental results of CoM tracking in the y direction. The figure shows the time history of CoM deviation from its initial position and linear momentum in each direction. The dashed lines indicate the references.

kinematics (IK). To make the problem even more interesting, we estimated the ground orientation using the on-board IMU with a PID control on $\mathsf{SO}(3)$ [47].

A preliminary walking experiment was also carried out to show the fundamental locomotion capability of BRUCE. The walking pattern generator is both kinematically and dynamically consistent, using MPC for the robot CoM based on LIPM [14] and cycloidal interpolation for the swing leg [19]. The planned trajectories are then tracked based on IK again. As in the supplementary video, with only open-loop control, BRUCE was able to walk a considerable amount.

C. Convex MHPC Evaluation

The convex MHPC framework discussed in Section III was implemented on BRUCE and the performance was evaluated in different scenarios. Note that for all the experiments, the optimal torque command solved by MHPC at first time step was directly sent to the robot.

1) Processing Time: The computation time of MHPC mostly depends on the number of DoFs of the robot, the number of contact vertices N_c, as well as the number of time steps into the future N_s. For BRUCE with 10 DoFs, 2 point contacts for each foot ($N_c = 4$), 5 time steps for simple model ($N_s = 5$ with $\Delta t = 0.1$ s), the processing time including problem formulation can achieve a frequency of 250 Hz using the off-the-shelf QP solver OSQP [48] on a laptop with an AMD Ryzen 5 4500U CPU at 2.1 GHz, which is sufficient for real-time feedback control.

2) Push Recovery: We are first interested in the balancing capability of MHPC as bipedal systems are intrinsically unstable. In this test, BRUCE was commanded to maintain its nominal standing posture. As shown in Fig. 8, an impulsive force was then exerted in the positive x direction followed by another one in the opposite direction. The push was forceful enough to immediately accelerate the robot CoM to around 0.1 m/s, but the robot managed to recover within the following two seconds. However, steady state error exists presumably due to model inaccuracy. Moreover, implementation of MHPC on BRUCE can also produce compliant behaviors thanks to its proprioceptive actuation. As in the supplementary video, when we pushed the robot with a constant force in various directions, it was able to react in a compliant manner and still keep its balance. Once we released the force, the robot went back to its original posture.

3) CoM Tracking: In the next experiment, BRUCE was commanded to perform a left-and-right shift motion, i.e., the robot CoM was tracking a sinusoidal curve of 0.5 Hz in the y direction, as shown in Fig. 9. We noticed that the robot was able to act in advance so as to minimize the overall tracking error since MHPC plans for the present moment while keeping future time slots in account.

4) Vertical Jumping: To demonstrate BRUCE's highly dynamic capability, a vertical jumping test was carried out finally. Though the robot was tracking a solely kinematically designed trajectory, it was still able to jump followed by the landing phase to mitigate the touchdown impact with the help of its proprioceptive actuation. We noticed that with a temporary lightweight upper body, the robot was not capable of stable and robust jumping motion because the rapid thigh movement would dominate, and the robot just flipped over, as in the supplementary video. We envision a much more powerful jump once a comparable upper body is added.

V. Conclusion and Future Work

This paper presents the development in design and control of BRUCE, a next-generation miniature bipedal robot. With the designed differential cable-driven pulley system and linkage mechanism, the distribution of leg mass and inertia is optimized in favor of dynamic behaviors. Proprioceptive actuation and contact sensing further enable BRUCE to safely interact with unstructured environments while providing rich feedback information. The proposed convex MHPC is able to plan and control dynamic motions in real time. The convex formulation is achieved by considering current states for the full-body model in the near horizon and linearizing the simple model in the long horizon. The preliminary testing results verify the basic functionalities of the robot design and explore its dynamic capabilities.

For future work, a comparable upper body will be designed to make BRUCE fully untethered. Meanwhile, the overall system will benefit from the upper body with the additional DoFs and more lumped inertia at the hip. The integration of a liquid cooling system into the actuators will also ensure steadier actuation performance. In addition, we are working on making BRUCE an open-source platform for the robotics community with an affordable cost below 6,500 USD. We envision it will boost humanoid studies as an accessible and reliable miniature humanoid robot platform.

REFERENCES

[1] Y. Sakagami *et al.*, "The intelligent asimo: system overview and integration," in *2002 IEEE/RSJ International Conference on Intelligent Robots and Systems (IROS)*, vol. 3, pp. 2478–2483 vol.3, 2002.

[2] M. Hutter *et al.*, "Anymal - a highly mobile and dynamic quadrupedal robot," in *2016 IEEE/RSJ International Conference on Intelligent Robots and Systems (IROS)*, pp. 38–44, 2016.

[3] X. Xiong and A. D. Ames, "Bipedal hopping: Reduced-order model embedding via optimization-based control," in *2018 IEEE/RSJ International Conference on Intelligent Robots and Systems (IROS)*, pp. 3821–3828, 2018.

[4] P. M. Wensing *et al.*, "Proprioceptive actuator design in the mit cheetah: Impact mitigation and high-bandwidth physical interaction for dynamic legged robots," *IEEE Transactions on Robotics*, vol. 33, no. 3, pp. 509–522, 2017.

[5] B. Katz, J. D. Carlo, and S. Kim, "Mini cheetah: A platform for pushing the limits of dynamic quadruped control," in *2019 International Conference on Robotics and Automation (ICRA)*, pp. 6295–6301, 2019.

[6] Y. Ding *et al.*, "Representation-free model predictive control for dynamic motions in quadrupeds," *IEEE Transactions on Robotics*, vol. 37, no. 4, pp. 1154–1171, 2021.

[7] https://www.bostondynamics.com/atlas.

[8] G. Ficht and S. Behnke, "Bipedal Humanoid Hardware Design: a Technology Review," *Current Robotics Reports*, vol. 2, pp. 201–210, June 2021.

[9] I. Ha *et al.*, "Development of open humanoid platform darwin-op," in *SICE Annual Conference 2011*, pp. 2178–2181, 2011.

[10] X. Zhang, *Application of Proprioception Quasi-Direct Drive Actuators on Dynamic Robotic Systems*. PhD thesis, UCLA, 2019.

[11] S. Kajita *et al.*, "Biped walking pattern generation by using preview control of zero-moment point," in *2003 IEEE International Conference on Robotics and Automation (ICRA)*, vol. 2, pp. 1620–1626, 2003.

[12] P. Wieber, "Trajectory free linear model predictive control for stable walking in the presence of strong perturbations," in *2006 6th IEEE-RAS International Conference on Humanoid Robots (Humanoids)*, pp. 137–142, 2006.

[13] A. Herdt *et al.*, "Online Walking Motion Generation with Automatic Foot Step Placement," *Advanced Robotics*, vol. 24, no. 5-6, pp. 719–737, 2010.

[14] S. Feng, X. Xinjilefu, C. G. Atkeson, and J. Kim, "Robust dynamic walking using online foot step optimization," in *2016 IEEE/RSJ International Conference on Intelligent Robots and Systems (IROS)*, pp. 5373–5378, 2016.

[15] H. Dai, A. Valenzuela, and R. Tedrake, "Whole-body motion planning with centroidal dynamics and full kinematics," in *2014 IEEE-RAS International Conference on Humanoid Robots*, pp. 295–302, 2014.

[16] S. Kuindersma *et al.*, "Optimization-based locomotion planning, estimation, and control design for the atlas humanoid robot," *Auton. Robots*, vol. 40, p. 429–455, Mar. 2016.

[17] J. Carpentier *et al.*, "A versatile and efficient pattern generator for generalized legged locomotion," in *2016 IEEE International Conference on Robotics and Automation (ICRA)*, pp. 3555–3561, 2016.

[18] J. Di Carlo *et al.*, "Dynamic locomotion in the mit cheetah 3 through convex model-predictive control," in *2018 IEEE/RSJ International Conference on Intelligent Robots and Systems (IROS)*, pp. 1–9, 2018.

[19] J. R. Hooks, *Real-Time Optimization for Control of a Multi-Modal Legged Robotic System*. PhD thesis, UCLA, 2019.

[20] S. Hong, J. Kim, and H. Park, "Real-time constrained nonlinear model predictive control on so(3) for dynamic legged locomotion," in *2020 IEEE/RSJ International Conference on Intelligent Robots and Systems (IROS)*, pp. 3982–3989, 2020.

[21] J. Shen and D. Hong, "A novel model predictive control framework using dynamic model decomposition applied to dynamic legged locomotion," in *2021 IEEE International Conference on Robotics and Automation (ICRA)*, pp. 4926–4932, 2021.

[22] J. Shen and D. Hong, "Convex model predictive control of single rigid body model on so(3) for versatile dynamic legged motions," in *2022 IEEE International Conference on Robotics and Automation (ICRA)*, 2022.

[23] J. Koenemann *et al.*, "Whole-body model-predictive control applied to the HRP-2 humanoid," in *2015 IEEE/RSJ International Conference on Intelligent Robots and Systems (IROS)*, pp. 3346–3351, 2015.

[24] M. Neunert *et al.*, "Whole-body nonlinear model predictive control through contacts for quadrupeds," *IEEE Robotics and Automation Letters*, vol. 3, no. 3, pp. 1458–1465, 2018.

[25] M. Posa, C. Cantu, and R. Tedrake, "A direct method for trajectory optimization of rigid bodies through contact," *The International Journal of Robotics Research*, vol. 33, no. 1, pp. 69–81, 2014.

[26] X. Lin, J. Zhang, J. Shen, G. Fernandez, and D. W. Hong, "Optimization based motion planning for multi-limbed vertical climbing robots," in *2019 IEEE/RSJ International Conference on Intelligent Robots and Systems (IROS)*, pp. 1918–1925, 2019.

[27] C. Mastalli *et al.*, "Crocoddyl: An efficient and versatile framework for multi-contact optimal control," in *2020 IEEE International Conference on Robotics and Automation (ICRA)*, pp. 2536–2542, 2020.

[28] J. Shen, Y. Liu, X. Zhang, and D. Hong, "Optimized jumping of an articulated robotic leg," in *2020 17th International Conference on Ubiquitous Robots (UR)*, pp. 205–212, 2020.

[29] J. Zhang, X. Lin, and D. W. Hong, "Transition motion planning for multi-limbed vertical climbing robots using complementarity constraints," in *2021 IEEE International Conference on Robotics and Automation (ICRA)*, pp. 2033–2039, 2021.

[30] H. Li, R. J. Frei, and P. M. Wensing, "Model hierarchy predictive control of robotic systems," *IEEE Robotics and Automation Letters*, vol. 6, no. 2, pp. 3373–3380, 2021.

[31] A. Tilley and H. Associates, *The Measure of Man and Woman: Human Factors in Design*. Interior design.industrial design, Wiley, 2001.

[32] T. Zhu, J. Hooks, and D. Hong, "Design, modeling, and analysis of a liquid cooled proprioceptive actuator for legged robots," in *2019 IEEE/ASME International Conference on Advanced Intelligent Mechatronics (AIM)*, pp. 36–43, 2019.

[33] https://westwoodrobotics.io/bearseries/koala-bear/.

[34] Y.-J. Kim, "Anthropomorphic low-inertia high-stiffness manipulator for high-speed safe interaction," *IEEE Transactions on Robotics*, vol. 33, no. 6, pp. 1358–1374, 2017.

[35] K. Kojima *et al.*, "A robot design method for weight saving aimed at dynamic motions: Design of humanoid jaxon3-p and realization of jump motions," in *2019 IEEE-RAS 19th International Conference on Humanoid Robots (Humanoids)*, pp. 586–593, 2019.

[36] https://www.agilityrobotics.com/robots.

[37] J. K. Salisbury *et al.*, "Compact cable transmission with cable differential," U. S. Patent 5 046 375, 1991-09-10.

[38] F. Nori *et al.*, "icub whole-body control through force regulation on rigid non-coplanar contacts," *Frontiers in Robotics and AI*, vol. 2, p. 6, 2015.

[39] J. Heinzmann and A. Zelinsky, "The safe control of human-friendly robots," in *1999 IEEE/RSJ International Conference on Intelligent Robots and Systems (IROS)*, pp. 1020–1025, 1999.

[40] B. G. Katz, "A low cost modular actuator for dynamic robots," Master's thesis, Massachusetts Institute of Technology, 2018.

[41] J. Yu *et al.*, "A proprioceptive, force-controlled, non-anthropomorphic biped for dynamic locomotion," in *2018 IEEE-RAS 18th International Conference on Humanoid Robots (Humanoids)*, pp. 1–9, 2018.

[42] R. Featherstone, *Rigid Body Dynamics Algorithms*. Berlin, Heidelberg: Springer-Verlag, 2007.

[43] M. Bloesch *et al.*, *State Estimation for Legged Robots: Consistent Fusion of Leg Kinematics and IMU*, pp. 17–24. MIT Press, 2013.

[44] S. K. Lam, A. Pitrou, and S. Seibert, "Numba: A llvm-based python jit compiler," in *2015 2nd Workshop on the LLVM Compiler Infrastructure in HPC*, 2015.

[45] J. C. Trinkle, J.-S. Pang, S. Sudarsky, and G. Lo, "On dynamic multi-rigid-body contact problems with coulomb friction," *ZAMM-Journal of Applied Mathematics and Mechanics/Zeitschrift für Angewandte Mathematik und Mechanik*, vol. 77, no. 4, pp. 267–279, 1997.

[46] P. M. Wensing and D. E. Orin, "Improved computation of the humanoid centroidal dynamics and application for whole-body control," *International Journal of Humanoid Robotics*, vol. 13, no. 01, p. 1550039, 2016.

[47] Z. Zhang, A. Sarlette, and Z. Ling, "Integral control on lie groups," *Systems & Control Letters*, vol. 80, pp. 9–15, 2015.

[48] B. Stellato *et al.*, "OSQP: an operator splitting solver for quadratic programs," *Mathematical Programming Computation*, vol. 12, no. 4, pp. 637–672, 2020.